JOURNAL OF ADVANCED DIELECTRICS
Vol. 10, No. 5 (2020) 2050021 (11 pages)

DOI: 10.1142/S2010135X20500216

The effect of Ba/Sr ratio on the Curie temperature for ferroelectric barium strontium titanate ceramics

Hamed A. Gatea*,†,§ and Iqbal S. Naji‡

*Al Ayen University, College of Health and Medical Technologies, Dhi-Qar, Iraq

†Dhi Qar Education Directorate, Nasiriyah, Dhi Qar Governorate, Iraq

‡University of Baghdad, Baghdad, Iraq

§hamedalwan14@gmail.com; hamed.alwan@alayen.edu.iq; gateahamed1966@gmail.com

Received 13 February 2020; Revised 20 August 2020; Accepted 25 August 2020; Published 10 October 2020

The powders of lead-free material namely (nonhazardous) barium strontium titanate (BST) with different stoichiometric compositions have been synthesized by the sol–gel method. $Ba_{1-x}Sr_xTiO_3$ (BST) materials possess the properties of both ferroelectric and dielectric materials. These materials have spontaneous polarization that can be reversed by an applied electric field and they remain polarized even when the applied external electric field is removed. Synthesized samples have been subjected to structural, morphological, and dielectric characterizations. In this study, BST nanopowders with different substitutions of x (where $x = 0.2$, 0.3, 0.4, 0.5, and 0.6) were prepared by the sol–gel method, which is an easy method with low power consumption and low temperature requirement and produces higher yield. Nanopowders had average particle sizes of 12–24 nm and particles sizes after sintering at 1000 °C for 3 h were 197, 267, 79.80, 63.09, and 63 nm. All resulting pellets had a polycrystalline structure. Crystal structure, space group, morphological characterization, and particle size were determined from the structural analysis using X-ray powder diffraction (XRD), energy-dispersive X-ray spectroscopy (EDX), and scanning electron microscopy (SEM). The dielectric measurements were made for BST pellets under different frequencies (1–200 kHz) from room temperature to 250 °C. The dielectric constants for the bulk were 743, 1566, 1091, 766, and 626 for $x = 0.2$, 0.3, 0.4, 0.5, and 0.6, respectively. From dielectric measurements, samples with $x = 0.2$ and 0.3 had the Curie temperatures of 70 °C and 28.5 °C, respectively, and remained intact below 0°C. The sample with $x = 0.3$ had a good dielectric measurement and moderate dissipation factor; it may be used in capacitance application as energy stores.

Keywords: Curie Temperature; dielectric constant; sol gel; $Ba_{1-x}Sr_xTiO_3$; perovskite structure.

1. Introduction

Ferroelectric materials are a special type of pyroelectric materials with the latter being a special type of piezoelectric materials, and all these types are classified as dielectric materials as shown in Fig. 1. Ferroelectric materials exhibit a spontaneous electric polarization below the Curie temperature (T_c).[1] Piezoelectric materials have the ability to generate electricity from applied mechanical stress and conversely, produce mechanical stress from the applied electric field.[2] Pyroelectric means heat-generated electricity.

This effect is also convertible as heat can be generated by electricity resulting from the change of state of electric polarization. The crystallographic structure of the material is related closely to piezoelectricity, pyroelectricity, and ferroelectricity phenomena. Indeed, the relation between these types of materials comes from the symmetry of their crystal structure.[1] Besides the classification of crystals into seven Bravais systems (14 lattices) according to their geometry, crystals are also classified into 32-point groups based on their symmetry with respect to points. Among the 32-point groups, 11 of them possess a center of symmetry and the remaining 21 are noncentrosymmetric. Piezoelectric crystals are those without centers of symmetry. These classes of crystals exhibit electric polarity when subjected to electric-field stress and strain. Among the 21 noncentrosymmetric point groups, 20 are classified as piezoelectric crystals. Polarization is a vector quantity, and the existence of spontaneous polarization in a crystal creates a unique direction or axis whereby the whole crystal is polarized.[2,3]

It has been reported that only 10 of the 20 piezoelectric crystal classes have unique polar axis and exhibit spontaneous polarization. These 10 polar crystal classes are often called the ferroelectric crystals.[3] Ferroelectric materials can be defined as dielectric materials with spontaneous polarization that can be reversed by an applied electric field and they remain polarized even after the external electric field is removed.[4,5] Ferroelectric materials exist in two phases: ferroelectric (polar) phase and paraelectric phase (nonpolar).[6] All ferroelectrics have a perovskite structure (ABO_3) as shown in Fig. 2, where A and B are atoms with different valence electrons and atomic radii.[7] More features

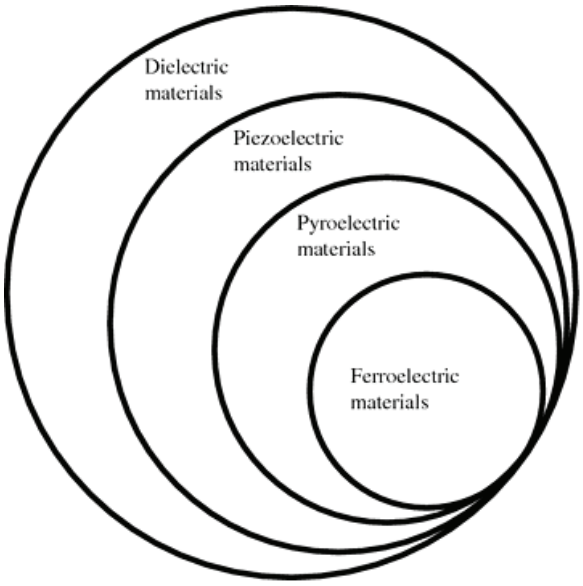

Fig. 1. The relation between all dielectric materials.[1]

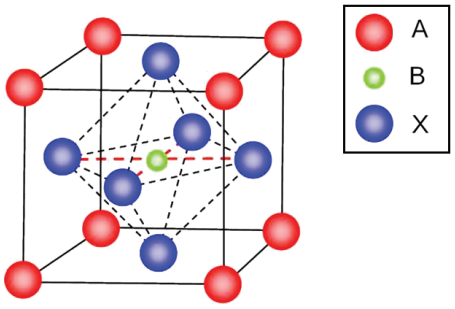

Fig. 2. Perovskite structure.[7]

can be seen in perovskite structure of barium strontium titanate (BST; $Ba_{1-x}Sr_xTiO_3$) compounds by substituting an atom of *A* for *B* or vice versa. When one ion is replaced with another ion, the properties for the compound such as conductivity or dielectric constant are changed.[7]

Curie temperature is the temperature at which maximum dielectric constant occurs and beyond this temperature polar materials change to nonpolar materials (ferroelectric to paraelectric materials).[9] Essential features of these materials have attracted attention because of their dielectric nonlinearity when a bias electric field is applied and their behavior is pronounced when their ratios of ions are manipulated, as they can have linearly adjustable Curie temperature.[6,10]

BST belong to the (ABO_3) perovskite family with a crystal structure of (ABX_3) and possesses similar crystalline properties to that of general perovskites which are cubic nature and have a chemical formula ($Ba_{1-x}Sr_xTiO_3$).[11,12] The perovskite structure of the BST compounds transition from the ferroelectric to paraelectric phase (cubic phase) is above the Curie temperature.[13] $Ba_{1-x}Sr_xTiO_3$ exhibits tetragonal and cubic phases depending on the Ba/Sr ratio and temperature. It has been observed that the ferroelectric state (tetragonal phase) is below the Curie temperature and the paraelectric state (cubic phase) is above the Curie temperature.[14]

There are different methods for preparing ferroelectrics powders. Preparation methods greatly affected the resulted materials. Among these methods is solid-state reaction which is considered as the conventional method for preparing a variety of nanopowders. The other method is freeze-drying, which is expensive and gives nanopowders.[15] The hydrothermal method is a chemical method carried out in solution media; the main feature of this method is its ability to give nanopowders with monosized particles.[16] There is also the sol–gel method, which is characterized by its ability to give more than one form or phase; these phases can be used for different subsequent preparations.[17]

The sol–gel method is one of the new, nonconventional methods for preparing metal oxide materials which are used in ceramic precursors, insulators, and catalyst support.[18] The use of the sol–gel method instead of the solid-state reaction method is because of a number of reasons. First, a nanoparticle can be obtained by controlling the preparation conditions such as the reflux time and the type of solvent used. Second, the solution is prepared at a low temperature, ranging from 60 °C to 120 °C.[19] Third, the sol–gel method has low sintering temperature compared to that of the solid-state reaction method as it does not exceed 1100–1150 °C, while that of solid-state reactions reaches 1450 °C.[20]

Ferroelectric materials are applied in various fields. The most important field of application is in the construction of component electronic devices such as capacitors, memories, transducers, and photonic devices, among others. Ferroelectric materials are also used in the communications industry and thermal photography (infrared photography). Dynamic random-access memory (DRAM), improvements in density, cost, speed, and immunity with scale are critical considerations for selecting a ferroelectric material. BST is a useful ferroelectric material for fabricating thin films used in DRAMs; moreover, BST can effectivity be used as storage dielectric materials in capacitors.[21]

2. Experimental Details

Many previous researchers have synthesized BST powders. Several factors influence the choice of an appropriate method for preparing BST ceramics, including cost, low temperature, and intended application. The raw materials used and the synthesis route followed affect the quality of the prepared powder. The sol–gel method has been used to synthesize the $Ba_{1-x}Sr_xTiO_3$ nanopowders with different ratios of Ba and Sr (x = 0.2, 0.3, 0.4, 0.5, and 0.6). Ba, Sr, and Ti used to form the compound were from salts such as barium acetate $Ba(CH_3CHOO)_2$ (99.5%; BDH Chemicals), strontium acetate $Sr(CH_3CHOO)_2$ (99%; Aldrich), and titanium(IV) isopropoxide (97%; Aldrich), respectively. Acetic acid

CH_3CHOOH (99.8%; Merck) was used as the solvent for the reaction mixture and 2-methoxyethanol as a stabilizer for titanium(IV) isopropoxide. First, the strontium acetate was dissolved in the acetic acid and a 2-M barium acetate solution of suitable volume and weight was prepared. Each solution was separately stirred at 60 °C for 60 min on a hotplate stirrer. These solutions were mixed and refluxed by a reflux system (Hotmintal [110 V], flask with three necks and a condenser) and the temperature of the solution was adjusted to 110 °C.

The solution was refluxed at 110 °C for 2 h until a transparent yellow solution was obtained. Then 2-methoxy ethanol (2–4 mL) was added to stabilize the crystal structure of titanium(IV) isopropoxide at room temperature. Barium acetate–strontium acetate mixture was titrated dropwise against the titanium(IV) isopropoxide solution. A buffering agent such as ammonium hydroxide was used to adjust the pH of the BST solution to 3–5. The mixture was refluxed again until a thick white gel was obtained.

A deionized water used to dilute the refluxed mixture and the final solution was stirred on a hot plate with a magnetic stirrer at 60 °C for 1 h. These steps were followed when preparing the various BST compositions. Finally, the solutions were dried at 200 °C for 2 h to evaporate the water completely for all the different compositions ($Ba_{0.8}Sr_{0.2}TiO_3$, $Ba_{0.7}Sr_{0.3}TiO_3$, $Ba_{0.6}Sr_{0.4}TiO_3$, $Ba_{0.5}Sr_{0.5}TiO_3$, and $Ba_{0.4}Sr_{0.6}TiO_3$). The powders were calcined at 700 °C for 2 h. The powders were then ground in a mortar to obtain a fine powder. BST nanopowders with fine powders were compacted in a cylindrical steel model with 120-mm internal diameter. The process was used to press the powder into pellets to reduce the vacancies in the porosity between the particles and shrink the particle size. The average particle dimensions were 120-mm diameter and 2.5–3-mm thickness under a converted pressure of 250–300 MPa. All pellets were sintered at 1000 °C for 3 h using a high-temperature programmable muffle furnace in an ambient atmosphere. A heat treatment cycle rate of 5 °C/min was developed to allow for better densification and to avoid cracking. Pellets were then cooled to room temperature (8 °C).

Field-emission scanning electron microscopy (FESEM; model Hitachi 4700) was used to study the surface morphology of the pellets. The composition properties of the pellets were studied using energy-dispersive X-ray spectroscopy (EDX). An X-ray diffractometer model (Bruker, Germany) with Cu-K_α radiation ($\lambda = 1.5418$ Å, 30 kV, and 30 mA), wide range of $2\theta = 20$–$80°$, and a scanning rate of 1 min^{-1} was used to determine the nanostructure of BST at room temperature.

3. Results and Discussion

The BST nanopowders prepared by the sol–gel method were characterized as perovskites. The composition and structural properties were examined through EDX, X-ray powder diffraction (XRD), and SEM images of the pellets. The dielectric constant and dissipation factor of both the bulk and thin film ferroelectric materials were recorded and the results analyzed. Microstructure, grain size, surface roughness, and phase content for the bulk played a key role in the electrical properties of pellets.

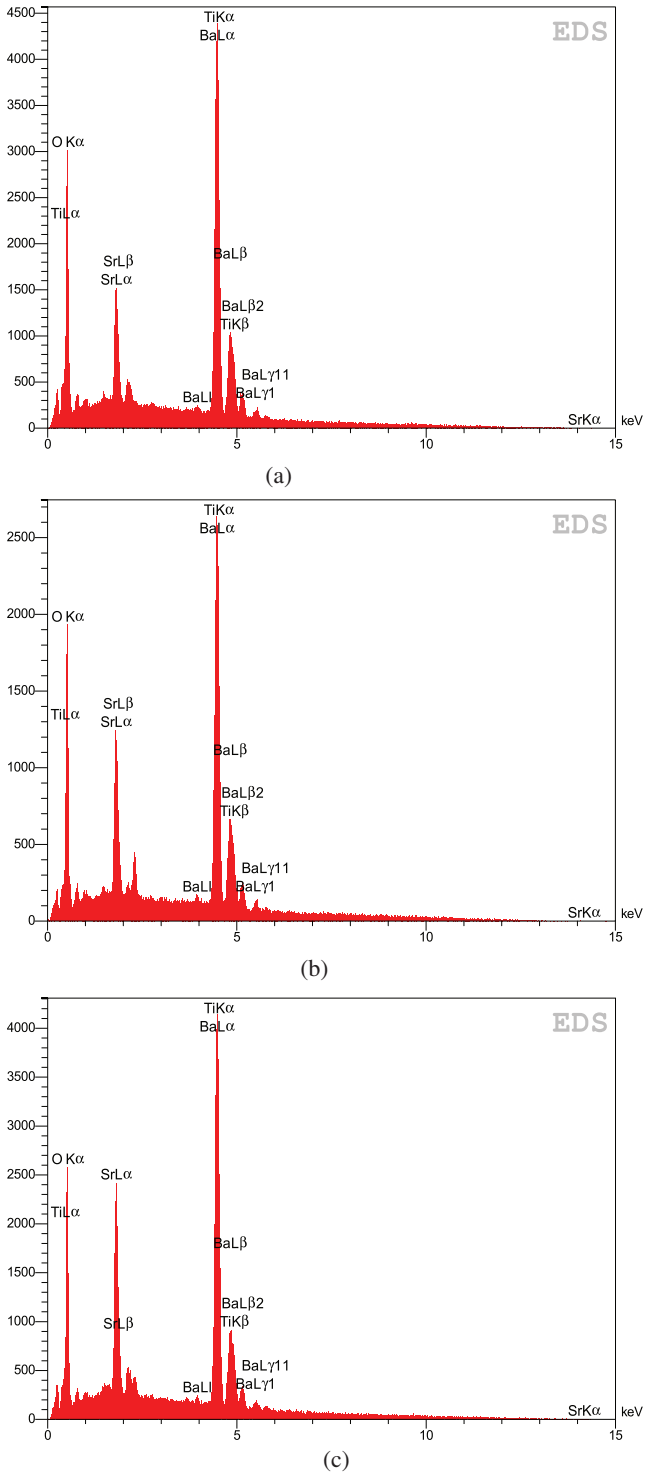

Fig. 3. EDX patterns of $Ba_{1-x}Sr_xTiO_3$ pellets with different x values: (a) $x = 0.2$, (b) $x = 0.3$, and (c) $x = 0.4$.

Table 1. The calculated and experimental values of the elements contained in the $Ba_{1-x}Sr_xTiO_3$ compound pellets.

x	Elements	Line	Standard values (wt.%)	Exp. values (wt.%)	Standard values (at.%)	Exp. values (at.%)
0.2	O	K_α	21.64	25.97	60	65.47
	Ti	K_α	21.59	22.55	20	18.99
	Sr	L_α	9.09	6.45	6.60	4.18
	Ba	L_α	47.68	45.03	13.40	11.36
0.3	O	K_α	22.14	20.3	60	59.32
	Ti	K_α	22.08	16.29	20	15.89
	Sr	L_α	13.34	16.58	4.60	8.85
	Ba	L_α	42.44	46.83	15.40	15.94
0.4	O	K_α	22.50	26.62	60	65.10
	Ti	K_α	22.44	22.58	20	18.47
	Sr	L_α	16.43	11.43	8	5.11
	Ba	L_α	38.63	39.37	12	11.32
0.5	O	K_α	23.04	26.56	60	64.56
	Ti	K_α	22.98	21.6	20	17.65
	Sr	L_α	21.03	19.19	10	8.53
	Ba	L_α	32.96	32.64	10	9.26
0.6	O	K_α	23.06	26.24	60	64.24
	Ti	K_α	23.54	22.57	20	18.45
	Sr	L_α	25.85	16.77	12	7.50
	Ba	L_α	27.01	34.42	8	9.82

3.1. *EDX analysis*

Figure 3 shows the EDX spectra of the bulk BST ($Ba_{1-x}Sr_xTiO_3$). The elements Ba, Sr, Ti, and O were observed. The dominant phase was the pure BST phase. Stoichiometric ratios of the main metallic elements of BST are shown in Table 1 as mass or atomic mass percentage. The stoichiometric composition of titanium and oxygen was approximately 1:3 for most of the samples. The stoichiometric composition of strontium and barium changed in relation to the value of x. The tendency of different samples for the experimental value in A% was different from the standard value in A% because of the different experimental conditions as portions of the solution were volatile and escaped from the beaker.

3.2. *XRD measurements*

Figure 4 shows the polycrystalline structure of the bulk $Ba_{1-x}Sr_xTiO_3$ with different x values were produced by the sol-gel method. Figure 4 shows that all the samples were polycrystals. The XRD patterns of $Ba_{0.8}Sr_{0.2}TiO_3$ and $Ba_{0.7}Sr_{0.3}TiO_3$ phases had many peaks that are related to the tetragonal perovskite phase along the (100), (101), (111), (200), (201), (211), (202), (221), and (301) planes. The peak positions of $Ba_{0.8}Sr_{0.2}TiO_3$ and $Ba_{0.7}Sr_{0.3}TiO_3$ matched well with the PDF Card Nos. 96-151-2121 and 00-044-0093, respectively. Furthermore, these phases exhibited the *P4mm* space group with $a = 3.9890$ Å and $c = 3.9950$ Å versus $a = 3.9771$ Å and $c = 3.9883$ Å, respectively.[19]

The XRD patterns of $Ba_{0.6}Sr_{0.4}TiO_3$, $Ba_{0.5}Sr_{0.5}TiO_3$, and $Ba_{0.4}Sr_{0.6}TiO_3$ phases showed nine peaks which corresponded to the (100), (110), (111), (200), (210), (211), (220), (221), and (310) planes. These peaks are related to the cubic BST

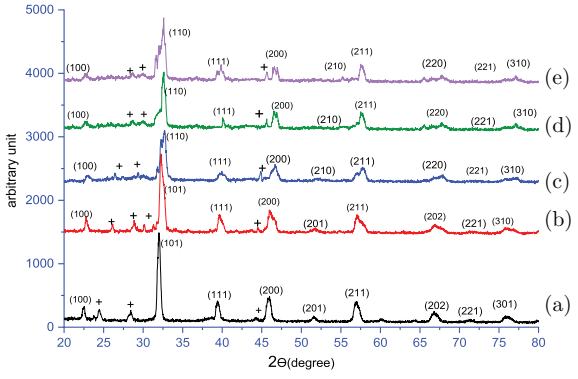

Fig. 4. XRD patterns of $Ba_{1-x}Sr_xTiO_3$ powders with various ratios of x sintered at 1000 °C: (a) $x = 0.2$, (b) $x = 0.3$, (c) $x = 0.4$, (d) $x = 0.5$, and (e) $x = 0.6$.

Table 2. Structural parameters viz. Miller indices, 2θ values, interplanar spacings, and phases of the $Ba_{1-x}Sr_xTiO_3$ powders.

$x = 0.2$									
hkl	100	101	111	200	201	211	202	221	301
$d_{Exp.}$ (Å)	3.9893	2.8232	2.3048	1.9962	1.7840	1.62835	1.4118	1.3301	1.2614
$d_{Stand.}$ (Å)	3.9890	2.8228	2.3042	1.9945	1.7839	1.6289	1.4114	1.3299	1.2616
2θ (Theo.)	22.33°	31.77°	39.10°	45.37°	51.12°	56.53°	66.18°	71°	75.16°
2θ (Exp.)	22.29°	31.67°	39.06°	45.37°	51.10°	56.44°	66.16°	70.89°	75.15°
$x = 0.3$									
hkl	100	101	111	200	201	211	202	221	310
$d_{Exp.}$ (Å)	3.9771	2.8122	2.2961	1.9885	1.7786	1.6215	1.4060	1.2576	1.2535
$d_{Stand.}$ (Å)	3.977	2.8162	2.2983	1.9885	1.7795	1.6246	1.4080	1.2610	1.2577
2θ (Theo.)	22.3357°	31.7474°	39.1636°	45.5816°	51.2988°	56.6061°	66.3277°	70.9422°	75.5339°
2θ (Exp.)	22.3363°	31.7481°	39.1642°	45.5621°	51.3012°	56.6100°	66.3281°	70.9431°	75.3203°
$x = 0.4$									
hkl	100	110	111	200	210	211	220	221	310
$d_{Exp.}$ (Å)	3.9600	2.8036	2.2891	1.9825	1.7732	1.6195	1.4018	1.3218	1.25401
$d_{Stand.}$ (Å)	3.9660	2.8060	2.2900	1.9823	1.7735	1.6190	1.4023	1.3213	1.2537
2θ (Theo.)	22.3984°	31.8658°	39.3113°	45.7322°	51.4850°	56.8005°	66.6377°	71.3196°	75.8175°
2θ (Exp.)	22.3991°	31.8666°	39.3124°	45.7332°	51.4865°	56.8024°	66.6371°	71.3118°	75.8211°
$x = 0.5$									
hkl	100	110	111	200	210	211	220	221	310
$d_{Exp.}$ (Å)	3.9470	2.7909	2.2788	1.9735	1.7651	1.6113	1.3954	1.2491	1.24897
$d_{Stand.}$ (Å)	3.9494	2.7918	2.2796	1.937	1.7649	1.6113	1.3954	1.2480	1.24804
2θ (Theo.)	22.4934°	32.0312°	39.4971°	45.9501°	51.7535°	57.1126°	67.0089°	71.6718°	76.2227°
2θ (Exp.)	22.4954°	32.0389°	39.4987°	45.9501°	51.7576°	57.1134°	67.0123°	71.6808°	76.2297°
$x = 0.6$									
hkl	100	110	111	200	210	211	220	221	310
$d_{Exp.}$ (Å)	3.9401	2.7886	2.2761	1.9630	1.7623	1.6097	1.3942	1.2465	1.2457
$d_{Stand.}$ (Å)	3.9394	2.7855	2.2744	1.9697	1.7617	1.6080	1.3927	1.2457	1.2537
2θ (Theo.)	22.5516°	32.1057°	39.5920°	45.0415°	51.8538°	57.2344°	67.1528°	71.8320°	76.3880°
2θ (Exp.)	22.5608°	32.1093°	39.5990°	45.0489°	51.8546°	57.2356°	67.1585°	71.8338°	76.3913°

phase and matched exactly with the PDF Card Nos. 00-034-0411, 00-039-1395, and 01-078-2723, respectively. The phases of BST compounds were transformed from the tetragonal phase (ferroelectric state) to the cubic phase (paraelectric state) when the concentration of Sr^+ ions was increased to 0.4, 0.5, and 0.6.

The interplanar spacings, Miller indices, and 2θ values of BST phases are shown in Table 2. These results agree with those of Refs. 5, 8, and 9. Figure 4 shows secondary phases besides the BST phase peaks that are represented by two weak diffractions at $2\theta = 28.8°$, 26.8°, and 24.2° for $BaTi_2O_5CO_3$, $BaTi_2O_5CO_3$, and $Ba_2Ti_2O_5CO_3$, respectively, and appeared as intermediate oxycarbonates. The impurities remained exhibited at 44.6° for the compound forms of Sr_2TiO_4, $SrTiO_{10}$, and $Sr_3Ti_2O_7$.[9,16,17] The peaks of the Sr^+ ion shifted toward higher 2θ angles as it has smaller radius (1.13 Å) than the Ba^+ ion (1.35 Å). The XRD patterns can be improved by increasing the sintering temperature as this leads to the disappearance of the secondary phases, this topic has been discussed in a previous study on these compounds.

3.3. *SEM analysis of powders*

Figure 5 shows the SEM photographs of the bulk $Ba_{1-x}Sr_xTiO_3$ samples for different x = 0.2, 0.3, 0.4, 0.5,

and 0.6. The reaction time for refluxing and stirring of the initial concentration greatly influence the particle size of the BST nanostructure. The particle size changes to 197, 267, 79.80, 63.09, and 46 nm for x = 0.2, 0.3, 0.4, 0.5, and 0.6, respectively. The particle size of BST decreases with an increase in Sr^{+} ions concentration because of the smaller radius of Sr^{+}. This result agrees with those of Refs. 15 and 17.

3.4. *Density measurements*

The parameters of density for the sintered samples were critical to the BST compounds. The densities of the samples were estimated from experimental parameters and calculated using the following equation[1]:

$$\rho = W/\text{thickness} \times \text{area} = W/V, \tag{1}$$

where ρ is the density (g/cm^3), W denotes the mass of the sample (g), and V is the volume of the sample (cm^3).

Theoretical density measurements were calculated using the equation[2]

$$\rho = M \times Z/V \times N_a, \tag{2}$$

where M is the molecular weight (g/mol), Z denotes the number of atoms per unit cell, and V is the unit cell volume.

The density of the sintered sample plays an important role in ceramics; the experimental densities were measured for the ceramic discs after sintering to measure the shrinkage volume because of the removal of porosity, i.e., densification. The experimental and theoretical densities for all the sintering samples were estimated accordingly and calculated using Eqs. (1) and (2). It is clear there are variations between the theoretical and experimental densities of the samples. As shown in Table 3, the densities decreased with increasing the value of x (i.e., as the Sr^{+} ions concentration increased) owing to Sr having a smaller radius than Ba. The relative density as a parameter was proportional between the theoretical and experimental densities.

3.5. *Dielectric measurements*

Figure 6 shows the dielectric constants as a function of frequency for BST pellets at different parameters and concentrations of x. There was a decrease in the dielectric constant with an increase in frequency up to 50 kHz, beyond which it fairly remained constant. At low frequencies, electronic, ionic, dipolar, and interfacial/surface polarizations contribute

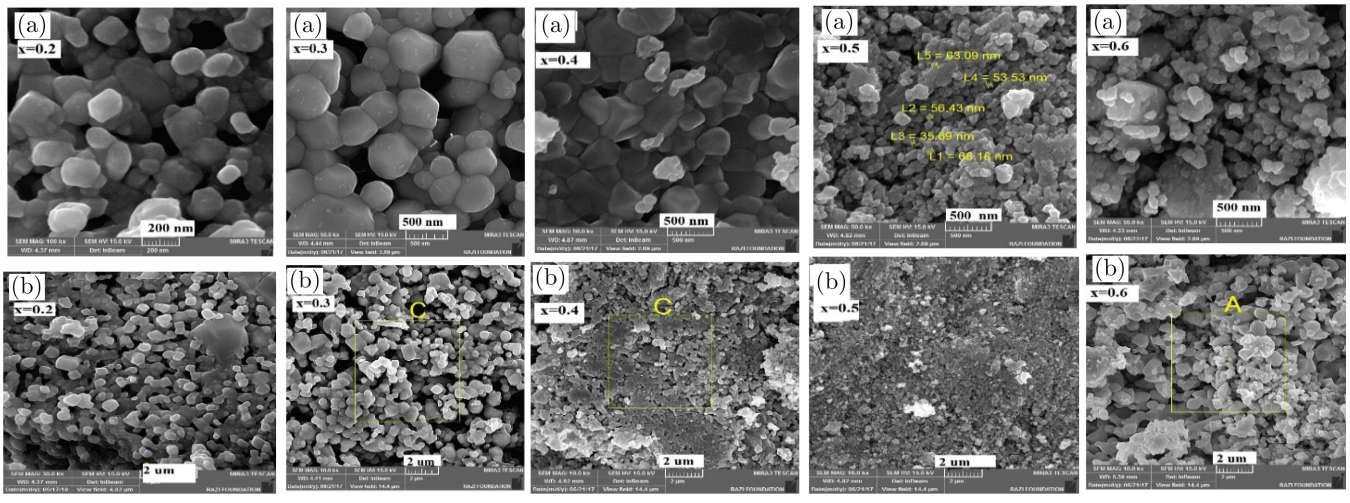

Fig. 5. FESEM images for the BST pellets with different x values which are sintered at 1000 °C.

Table 3. The densities of BST pellets for different x values after sintering at 1000 °C for 3 h.

Sample	$Ba_{0.8}Sr_{0.2}TiO_3$	$Ba_{0.7}Sr_{0.3}TiO_3$	$Ba_{0.6}Sr_{0.4}TiO_3$	$Ba_{0.5}Sr_{0.5}TiO_3$	$Ba_{0.4}Sr_{0.6}TiO_3$
Substitution factor (x)	0.2	0.3	0.4	0.5	0.6
Geometrical density (g/cm^3)	4.71	4.83	4.12	3.74	3.44
Theoretical density (g/cm^3)	5.83	5.74	5.66	5.59	5.43
Relative density (%)	80.78902	84.1463	72.79151	66.9051	63.1933
Porosity	19.21	15.854	27.20849	33.049	36.8067

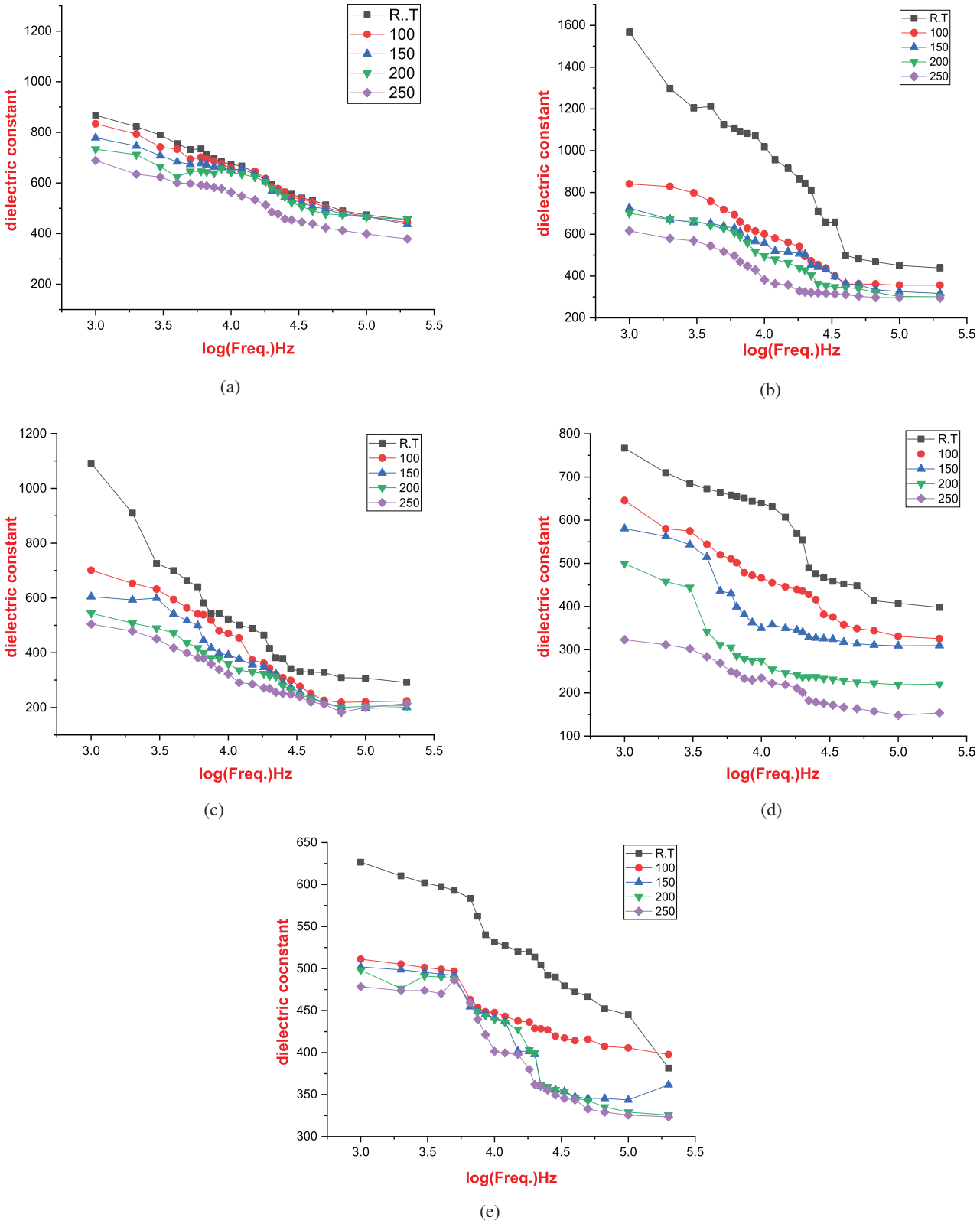

Fig. 6. Dielectric constants for BST pellets versus the frequency at different temperatures for different x values: (a) $x = 0.2$, (b) $x = 0.3$, (c) $x = 0.4$, (d) $x = 0.5$, and (e) $x = 0.6$.

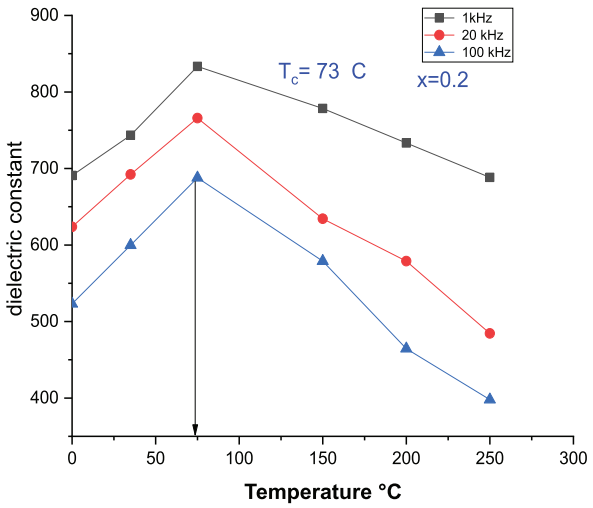

(a)

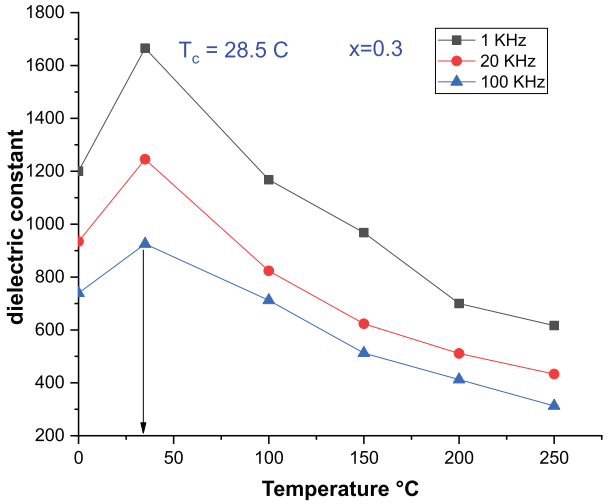

(b)

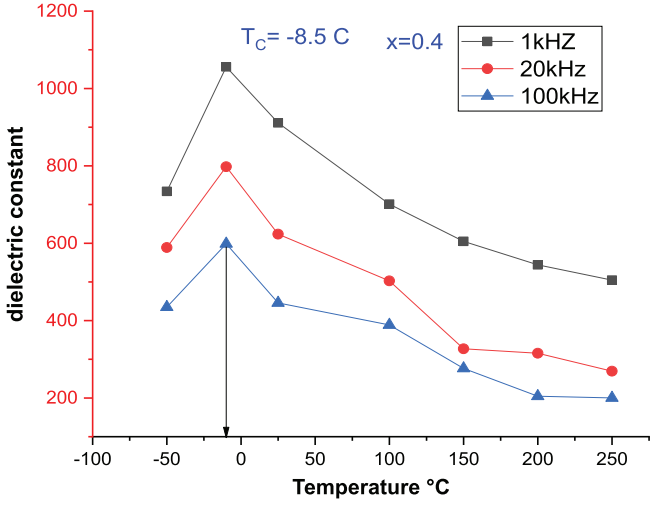

(c)

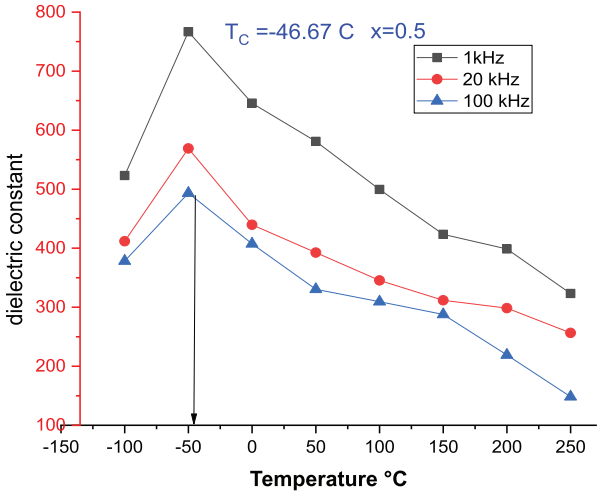

(d)

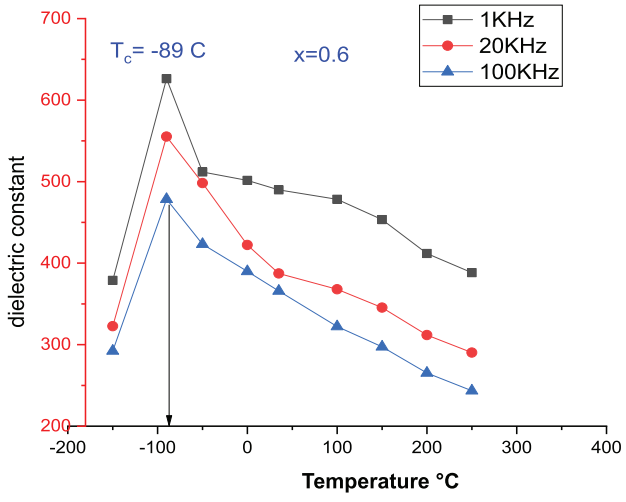

(e)

Fig. 7. Dielectric constants of BST pellets versus the temperature at different x values for different frequencies: (a) $x = 0.2$, (b) $x = 0.3$, (c) $x = 0.4$, (d) $x = 0.5$, and (e) $x = 0.6$.

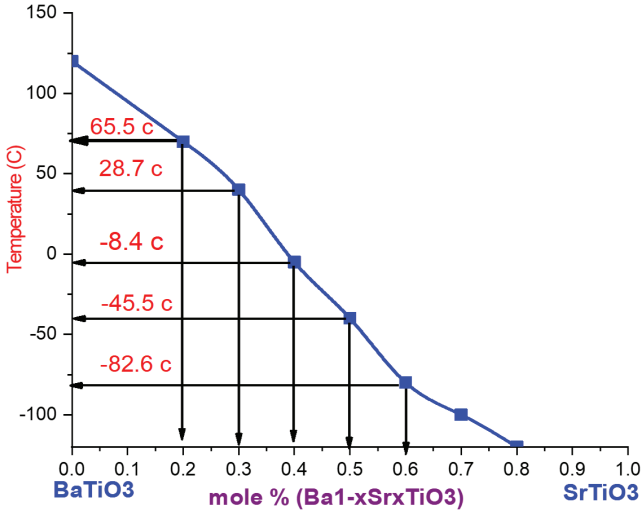

Fig. 8. Curie temperatures of transition for the BST samples at different values of x; at Curie temperature, the ferroelectric phase transitions into paraelectric phase.

to the total value of the dielectric constant, but for frequencies above 50 kHz, the contribution from interfacial/surface polarization is minimized.

In Fig. 7, the dielectric constants are plotted as a function of temperature. It was clear that the dielectric constants decreased with increasing temperature above the Curie temperature. For an increase below the Curie temperature, the dielectric constants decreased leading to an increase in conductivities. The conductivities increased with increasing frequency because of the vibrations of lattices that led to the vibration of atoms or molecules around their sites which caused the excitation of atoms. Frequencies that are responsible for increased conductivities and reduced dielectric constants may be provided by the product carriers.

Sample (x = 0.2) had a Curie temperature of approximately 70 °C; first, the sample below Curie temperature had a ferroelectric state which in turn exhibited spontaneous polarization. The dielectric constant increased initially until it reached the Curie point. Then the dielectric constant attained the maximum peak and then decreased with increasing temperature because of the transition to a paraelectric phase which does not have a spontaneous polarization.

A gradual decrease in the dielectric constants was noticed with increasing value of x; increasing the value of x from 0.2 to 0.6 led to changes in the densities of samples and increase in the porosities. The mixture gave reduced values of the dielectric constants.

Figure 9 illustrates the dissipation factors versus temperature, and there was not regular behavior when the temperature was increased. The dissipation factor mostly increased with increasing temperature. Low dissipation factors were exhibited at $x = 0.3$ and 0.5 and different values were observed for the remaining samples. The explanation for the sample with $x = 0.3$ is because of its high density owing to its large particle size, as shown in the SEM images.

As shown in Table 4, it is obvious that concerning the dielectric constants of BST pellets with different x values at 1 kHz and 100 kHz, the maximum dielectric constant was exhibited at $x = 0.3$ and this is attributable to the large grain size as shown in the SEM images. Moreover, dielectric constants decreased with increasing value of x, because of the decrease in the density when the ratio of x increases. This case revealed that $x = 0.3$ would be suitable for many applications such as energy storage or DRAM as it has a high dielectric

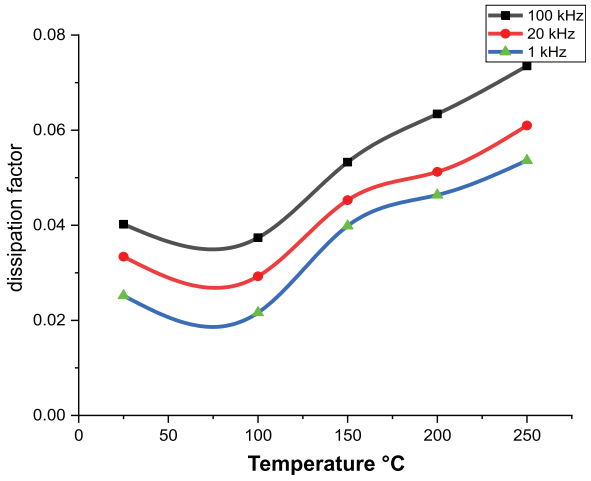

(a)

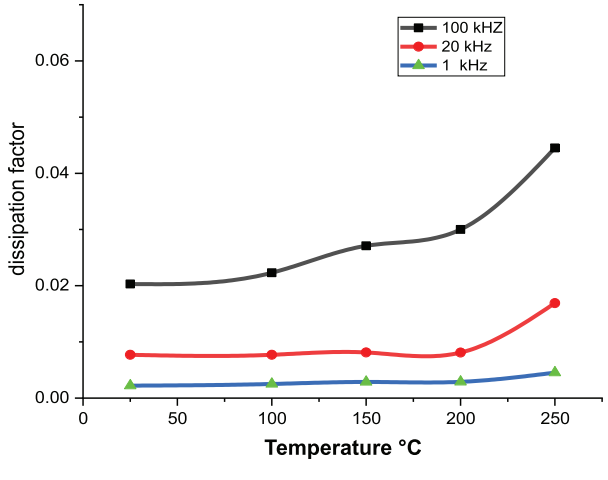

(b)

Fig. 9. Dissipation factors for the BST pellets versus the temperature at different x values for different frequencies: (a) $x = 0.2$, (b) $x = 0.3$, (c) $x = 0.4$, (d) $x = 0.5$, and (e) $x = 0.6$.

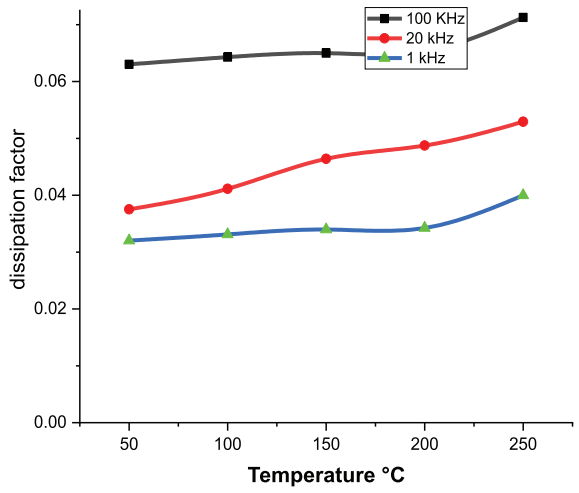

(c)

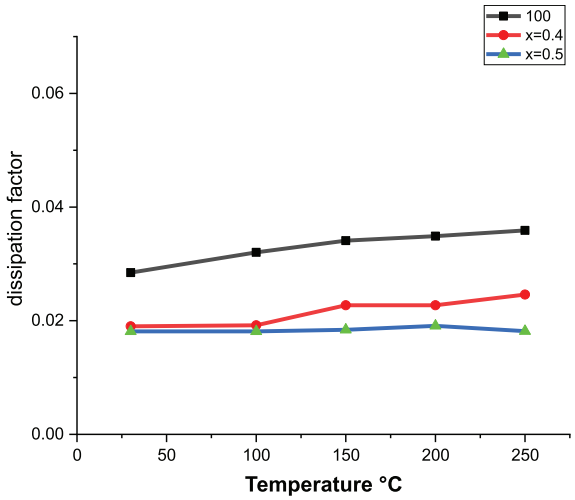

(d)

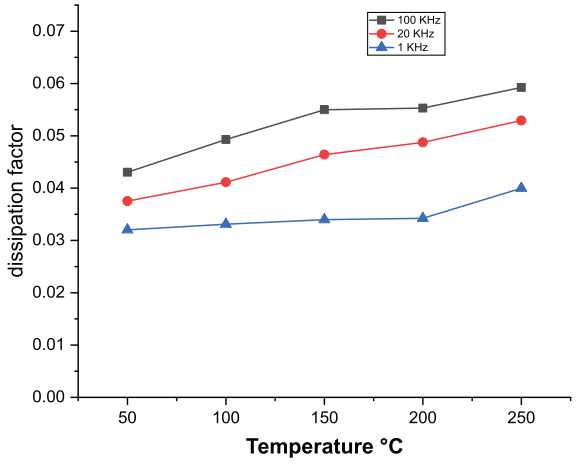

(e)

Fig. 9. (*Continued*)

Table 4. The values of dielectric constant with different x values at different temperatures at the two frequencies of 1 kHz and 100 kHz.

Dielectric constant 1 kHz					
T(°C)	$x = 0.2$	$x = 0.3$	$x = 0.4$	$x = 0.5$	$x = 0.6$
R.T	743.37	1566.876	1091.67	766.65	626.52
100	711.37	840.725	701.02	645.50	511.164
150	678.7	725.4301	604.82	580.57	501.942
200	622.287	699.808	544.072	499.60	489.145
250	589.77	616.59	504.51	323.29	478.378
Dielectric constant 100 KHz					
R.T	422.76	450.3592	307.3856	407.6657	444.9823
100	467.387	356.3757	220.7571	330.944	405.5682
150	467.368	325.6245	196.9076	309.2263	343.5487
200	464.487	302.1312	204.4838	218.9634	329.1373
250	398	296.1395	200.3431	148.2864	325.6299

constant, which gives it a high storage energy density and makes it suitable for use as a capacitor in integrated circuits.

BST can be in either tetragonal or cubic symmetry ($BaTiO_3$ is ferroelectric at room temperature whereas $SrTiO_3$ is a paraelectric) depending upon the Ba/Sr ratio and temperature. At temperatures above the phase transition temperature, T_c, the material is in cubic paraelectric state — it does not have spontaneous polarization, while below T_c, the material exhibits tetragonal ferroelectric state — it has spontaneous polarization. The lattice parameters and T_c depend on the Ba/Sr ratio.

Curie temperature depends on the composition of strontium and large polarizations and permittivities, its known properties are basically influenced by the temperature in perovskite structure-type materials. The ferroelectric phase switched to the paraelectric phase at Curie temperature. Curie temperature decreased linearly with increasing Sr^+ ions concentration, i.e., $Ba_{0.8}Sr_{0.2}TiO_3$ (70 °C), $Ba_{0.7}Sr_{0.3}TiO_3$ (28.7 °C), $Ba_{0.6}Sr_{0.4}TiO_3$ (−8.4°C), $Ba_{0.5}Sr_{0.5}TiO_3$ (−45.5 °C), and $Ba_{0.4}Sr_{0.6}TiO_3$ (−82.6 °C), as shown in Fig. 8.

4. Conclusion

$Ba_{1-x}Sr_xTiO_3$ compounds were prepared by the sol–gel method with different values of x = 0.2, 0.3, 0.4, 0.5, and 0.6. When Sr^+ ions concentration was increased, the density of the samples decreased because of the small radius of Sr^+. Electrical property such as Curie temperature exhibited variations depending on the Ba/Sr ratio. When the ratio was adjusted with different Sr concentrations, Curie temperature decreased with increasing Sr^+ ions concentration. The samples with x = 0.2, 0.3, 0.4, 0.5, and 0.6 exhibited Curie temperatures of 70 °C, 28.7 °C, −8.4 °C, −45.5 °C, and −82.6 °C, respectively. The result of the XRD analysis confirms the formation of BST phase samples. The phases of $Ba_{0.8}Sr_{0.2}TiO_3$ and $Ba_{0.7}Sr_{0.3}TiO_3$ were found to be tetragonal and the remaining samples ($Ba_{0.6}Sr_{0.4}TiO_3$, $Ba_{0.5}Sr_{0.5}TiO_3$, and $Ba_{0.4}Sr_{0.6}TiO_3$) appeared in the cubic phase. The FESEM images of samples sintered at 1000 °C showed good surface morphology and average grain sizes of 197, 267, 79.08, 63.09, and 46 nm for the different values of x = 0.2, 0.3, 0.4, 0.5, and 0.6, respectively. The density of samples decreased with an increased value of x for the $Ba_{1-x}Sr_xTiO_3$ compounds. Furthermore, the relative density decreased with an increased value of x.

The dielectric constants decreased with increasing frequencies. Owing to the temperature dependence of dielectric constant at different compositions, the dielectric constant decreased with increasing the temperature above the Curie temperature and increased below the Curie temperature. Dissipation factor was calculated for the samples sintered at 1000 °C. The dissipation factor was dependent on temperature for all the samples, it increased when increasing the temperature. From the above, it can be noted that the best capacitors were made up of x = 0.3 for the pellets as they had a good high dielectric constant and a suitable dissipation factor.

Acknowledgments

The authors thank all the persons who helped them complete this work.

Conflict of Interest

The authors declare no competing financial interest.

References

[1]B. M. Natheer, Preparation and characterization of ferroelectric compound like $Ba_xSr_{1-x}TiO_3$, Ph.D. thesis, Al-Nahrain University, Iraq (2012).
[2]L. Guo, H. Luo, J. Gao, L. Guo and J. Yang, Microwave hydrothermal synthesis of barium titanate powders, *Mater. Lett.* **60**, 3011 (2006).
[3]A. K. Bain and P. Chand, *Ferroelectrics: Principles and Applications*, 1st edn. (Wiley-VCH Verlag Gmbh & Co., Weinheim, 2017).
[4]A. K. Bain and P. Chand, *Ferroelectrics: Principles and Applications*, 1st edn. (Wiley-VCH, 2017).
[5]G. S. Kathait, V. Rohilla, P. Thapliyal, D. Biswas and S. Singh, Effect of different strontium content on dielectric properties of barium strontium titanate ceramic, *Int. J. Latest Technol. Eng. Manage. Appl. Sci.* **VI**, 75 (2017).
[6]S. Agarwal, Preparation and characterization of barium strontium titanate ceramics by gel-combustion technique, B.Tech. thesis, National Institute of Technology, Rourkela, Odisha (2013).
[7]K. Uchino, *Ferroelectric Devices*, 2nd edn. (CRC Press, 2010).
[8]M. Niederberger, G. Garnweitner, N. Pinna and M. Antonietti, Nonaqueous and halide-free route to crystalline $BaTiO_3$, $SrTiO_3$, and (Ba, Sr)TiO_3 nanoparticles via a mechanism involving C–C bond formation, *J. Am. Chem. Soc.* **126**, 9120 (2017).
[9]V. Somani and S. J. Kalita, Synthesis and characterization of nanocrystalline barium strontium titanate powder via sol-gel processing, *J. Electroceramics* **18**, 57 (2007).
[10]A. Ioachim, M. I. Toacsan, M. G. Banciu, L. Nedelcu, A. Dutu, S. Antohe, C. Berbecaru, L. Georgescu, G. Stoica and H. V. Alexandru, Transitions of barium strontium titanate ferroelectric ceramics for different strontium content, *Thin Solid Films* **515**, 6289 (2007).
[11]K. Verma, S. Sharma, D. K. Sharma, R. Kumar and R. Rai, Sol-gel processing and characterization of nanometersized (Ba,Sr)TiO_3 ceramics, *Adv. Mater. Lett*. **3**, 44 (2012).
[12]J. V. Mantese and S. Pamir Alpay, *Graded Ferroelectrics, Transpacitors and Transponents*, Chapter 2 (Springer Science+Business Media, USA, 2005), p. 48.
[13]H. Xu, L. Gao and J. Guo, Preparation and characterizations of tetragonal barium titanate powders by hydrothermal method, *J. Eur. Ceram. Soc.* **22**, 1163 (2002).
[14]C. Mao, S. Yan, S. Cao, C. Yao, F. Cao, G. Wang, X. Dong, X. Hu and C. Yang, Effect of grain size on phase transition, dielectric and pyroelectric properties of BST ceramics, *J. Eur. Ceram. Soc.* **34**, 2933 (2014).
[15]Y. Gao, V. V. Shvartsman, D. Gautam, M. Winterer and D. C. Lupascu, Nanocrystalline barium strontium titanate ceramics synthesized via the 'organosol' route and spark plasma sintering, *J. Am. Ceram. Soc*. **97**, 2139 (2014).
[16]H. A. Gatea and I. S. Naji, Preparation and characterization of $Ba_{1-x}Sr_xTiO_3$ by sol-gel method, *Asian J. Chem.* **31**, 186 (2018).
[17]M. E. Azim Araghi, N. Shaban and M. Bahar, Synthesis and characterization of nanocrystalline barium strontium titanate powder by a modified sol-gel processing, *Mater. Sci*. **34**, 63 (2016).
[18]H. A. Gatea and I. S. Naji, Impact of sintering temperature on structural and dielectric properties of barium strontium titanate, *J. Ovonic Res.* **14**, 467 (2018).
[19]C. Zhang, Z.-X. Ling, G. Jian and F.-X. Chen, Dielectric properties and point defect behavior of antimony oxide doped Ti deficient barium strontium titanate ceramics, *Trans. Nonferr. Met. Soc. China* **27**, 2656 (2017).
[20]C. F. H. He, W. Cai, R. Gao and G. Chen, Effects of sintering temperature on density, *Advanced Functional Materials* **32**, 32 (2018).
[21]Z.-G. Ye (ed.), *Handbook of Advanced Dielectric, Piezoelectric and Ferroelectric Materials: Synthesis, Properties and Applications* (Woodhead Publishing Limited, 2008).